

A modeling study of an East Asian convective complex during March 2001

Matthew H. Hitchman, Marcus L. Buker, and Gregory J. Tripoli

Department of Atmospheric and Oceanic Sciences, University of Wisconsin-Madison, Madison, Wisconsin, USA

R. B. Pierce, J. A. Al-Saadi, E. V. Browell, and Melody A. Avery

NASA Langley Research Center, Hampton, Virginia, USA

Received 31 October 2003; revised 8 March 2004; accepted 9 April 2004; published 7 July 2004.

[1] During March–April 2001 the University of Wisconsin Nonhydrostatic Modeling System (UWNMS) was used to provide flight planning and estimation of ozone flux into the troposphere over East Asia in support of the Transport and Chemical Evolution over the Pacific (TRACE-P) mission. On 24 March a convective complex developed in eastern China and propagated eastward over the Pacific south of Japan. Aircraft and satellite observations, together with the UWNMS simulations, captured this convective event, which first entrained urban boundary layer air over Asia and then marine boundary layer air over the Pacific. The convective updraft split the subtropical westerly jet, deformed the tropopause upward, radiated gravity waves into the stratosphere, and induced a ring of stratospheric ozone to descend around its periphery into the middle troposphere. The DC-8 observations and UWNMS show a vault of moderate ozone (~ 65 ppbv) in the 8–12 km layer within the convection, with high stratospheric values (~ 100 ppbv) subsiding around the periphery into the troposphere near 6.5 km. A new two-scale method for diagnosing cross-tropopause ozone flux is compared with an annular volume estimate. During this 24 hour convective event, ~ 0.8 Tg ozone entered the troposphere from the stratosphere, comparable in magnitude to ozone fluxes in midlatitude cyclones. *INDEX TERMS*: 0320 Atmospheric Composition and Structure: Cloud physics and chemistry; 0341 Atmospheric Composition and Structure: Middle atmosphere—constituent transport and chemistry (3334); 0368 Atmospheric Composition and Structure: Troposphere—constituent transport and chemistry; 0365 Atmospheric Composition and Structure: Troposphere—composition and chemistry; *KEYWORDS*: ozone transport, stratosphere-troposphere exchange

Citation: Hitchman, M. H., M. L. Buker, G. J. Tripoli, R. B. Pierce, J. A. Al-Saadi, E. V. Browell, and M. A. Avery (2004), A modeling study of an East Asian convective complex during March 2001, *J. Geophys. Res.*, 109, D15S14, doi:10.1029/2003JD004312.

1. Introduction

[2] A primary goal of the Transport and Chemical Evolution over the Pacific (TRACE-P) mission over East Asia during March and April 2001 was to quantify the contribution of stratospheric ozone to observed tropospheric ozone [Jacob *et al.*, 2003]. East Asia is both a strong source of anthropogenic compounds and a preferred location for cyclogenesis and descent of ozone from the stratosphere [e.g., Danielsen *et al.*, 1987]. The convective complex which developed over China on 24 March was sampled in detail by DC-8 measurements on flight 14 and simulated with the University of Wisconsin Nonhydrostatic Modeling System (UWNMS). Strong downwelling of stratospheric ozone into the troposphere occurred around the periphery of the convection. This paper presents a case study of this storm and applies a new two-scale method for estimating

ozone flux across the tropopause. Kittaka *et al.* [2004] examined the sulfur budget of this storm. M. L. Buker *et al.* (Resolution dependence of cross-tropopause ozone transport over East Asia, submitted to *Journal of Geophysical Research*, 2004, hereinafter referred to as Buker *et al.*, submitted manuscript, 2004) applied the two-scale method to a synoptic cyclone event during TRACE-P on 26 March 2001.

[3] Pierce *et al.* [2003] used the method of Wirth and Egger [1999] to calculate the ozone budget for the 37 days of the TRACE-P mission (7 March to 12 April) using the Regional Air Quality Modeling System (RAQMS) with online chemical calculations. The RAQMS combines the fidelity of global isentropic transport with high regional resolution from the UWNMS component. Using a 6600×4500 km domain with 110 km resolution, they found that the daily average flux of ozone from the stratosphere into the domain troposphere was ~ 0.22 Tg d^{-1} , exceeding net production minus loss in the domain (~ -0.17 Tg d^{-1}) by 0.05 Tg d^{-1} . Ozone flow out the eastern boundary of

$\sim -5.25 \text{ Tg d}^{-1}$ [cf. *Browell et al.*, 2003] exceeded ozone flow in from the south, west, and north by $\sim 0.03 \text{ Tg d}^{-1}$.

[4] Although current models seem to estimate cross-tropopause ozone flux reasonably well, a conceptual gap exists between how models simulate this process and what is believed to be occurring. The extratropical tropopause may be characterized by a rapid upward increase in potential temperature or PV. In the absence of diabatic processes, the tropopause is a material surface. Theory holds that air can flow across the tropopause only if there is diabatic heating or irreversible mixing [e.g., *Haynes and McIntyre*, 1990]. Atmospheric flow at scales larger than the Rossby radius is fundamentally nondivergent, with rotational flow advecting constituent fields along with the tropopause. Inviscid advection would produce folding but yield no transport across it. Yet observations suggest that smaller-scale chaotic mixing, gravity waves, inertial and convective instability, turbulence, radiative damping, and other diabatic and viscous processes enable ozone to cross the tropopause. In contemporary grid point models, ozone flux is the result of parameterized diffusion, usually with constant coefficient and exponent, and resolved net heating. For air to cross isentropic surfaces it must experience net heating. Thus grid-resolved net heating provides an estimate of cross-tropopause flux, but its accuracy is limited by vertical resolution. Photon exchange between rapidly evolving adjacent thermal perturbations increases quickly with reduced scale [*Haynes and Ward*, 1993] and can be much larger than climatological net heating rates near the tropopause, which are typically less than 0.5 K d^{-1} [e.g., *Kiehl and Solomon*, 1986; *Shine*, 1987].

[5] Most models' average temperatures and winds agree reasonably well with observations. Since parameterized diffusion and grid-resolved heating help determine their distribution, this suggests that ozone fluxes evaluated this way are probably the right order of magnitude. Nevertheless, it would be desirable to have a more physically based representation of cross-tropopause flux which can vary according to local motions in the model. Many models, including the UWNMS, explicitly represent motions at scales from tens to hundreds of kilometers, which can contribute toward irreversible exchange across the tropopause. This motivated developing a new diagnostic tool for assessing ozone flux, which utilizes model-resolved meso-scale motions.

[6] The two-scale method is based on observations which show that at scales longer than the Rossby radius (a few hundred kilometers) the flow is primarily advective, while on smaller scales the flow is characterized by folding and stretching, with filamentous intrusion leading to irreversible mixing [e.g., *Shapiro*, 1980; *Hoskins et al.*, 1985; *Danielsen et al.*, 1987; *Reid and Vaughan*, 1991; *Holton et al.*, 1995; *Haynes and Anglade*, 1997; *Sato and Dunkerton*, 2002]. The total wind field, \mathbf{V} , is divided into a "smoothed wind field," \mathbf{V}_s , which is assumed to be purely advective, and the remainder is the "mixing wind field," $\mathbf{V}_m = \mathbf{V} - \mathbf{V}_s$, which is assumed to cause irreversible mixing. A biharmonic 1-2-1 spatial filter is applied m times to achieve a low-pass filter with frequency response $R_m = \cos^{2m}(\frac{\pi \delta x}{L})$, where δx is the grid resolution, and L is a chosen scale. The frequency response varies slowly, such that contributions to the mixing wind decrease gradually toward larger scales. For application to

the 24 March event we chose a low-pass smoothing function which retained 60% of the wind at 1000 km scale and 10% at 500 km scale. The PV tropopause is calculated from the smoothed wind field, and its motion is given by $(\mathbf{V}_s \cdot \hat{n})\hat{n}$, where $\hat{n} = \nabla P_s / |\nabla P_s|$ is the normal to the tropopause. High-resolution ozone and mixing winds are used to calculate the flux of ozone across the tropopause: $\mathbf{F} = \chi_{\text{O}_3}(\mathbf{V}_m \cdot \hat{n})\hat{n}$, where χ_{O_3} is ozone number density.

[7] This method can be applied to the flux of any constituent across any chosen surface. Calculation of flux convergences provides the transport component for a constituent budget. This practical diagnostic tool, based on deduction of a gradual dynamical transition across $\sim 500 \text{ km}$ horizontal scale, provides a means of calculating ozone flux at each model grid point based on the strength of mixing winds. Here an upper bound on flux across the tropopause is given by using resolved model winds and assuming that filamentous intrusions are irreversible.

[8] *Buker et al.* (submitted manuscript, 2004) applied the two-scale method in the UWNMS to the case of DC-8 flight 15 on 26 March 2001, which was characterized by a strongly filamented jet and developing cyclone. They tested the dependence of ozone flux on model resolution, degree of smoothing of the wind field, and PV level. In this paper we highlight the importance of convective complexes for stratosphere-troposphere exchange (STE) and apply the two-scale method to the convective event of 24 March.

[9] Section 2 describes the UWNMS, TRACE-P forecasts, and observations used in this study. The UWNMS forecast of the convective complex is described in section 3. Aircraft observations are described in section 4. A higher-resolution simulation of this event is compared with these observations in section 5, which includes estimation of ozone transport near the convection. A summary is given in section 6.

2. UWNMS Forecasts and TRACE-P Observations

2.1. UWNMS Applications

[10] The UWNMS was initially designed to study tropospheric-scale interaction problems. It includes multiple interactive grid nesting, tropospheric microphysics, radiative transfer, and surface processes. It has been applied to tropical cloud clusters, hurricanes, midlatitude cyclones, polar lows, gravity waves, lake effect snow storms, and mesoscale convective complexes [*Tripoli*, 1992a, 1992b; *Pokrandt et al.*, 1996; *Mecikalski and Tripoli*, 1997; *Avissar et al.*, 1998]. The UWNMS has been adapted for application to transport problems involving the troposphere and lower stratosphere. *Hitchman et al.* [1999] found that synoptic waves effectively transport ozone out of the arctic stratosphere, contributing significantly to the observed decline of column ozone during summer. During December 1999 to March 2000 a variety of polar stratospheric clouds (PSCs) were found in the Arctic. The DC-8 observations and UWNMS simulations showed that the PSCs in December 1999 were due to inertia-gravity waves radiating into the cold pool from the adjusting tropopause polar front jet [*Hitchman et al.*, 2003]. The UWNMS has been combined with a global isentropic model [*Johnson et al.*, 1993] and the Langley online chemistry package [*Eckman et al.*, 1995]

to create the RAQMS [Pierce et al., 2003; Kittaka et al., 2004].

2.2. TRACE-P Forecasts

[11] The TRACE-P campaign included instrumented flights from Hong Kong and Yokota, Japan, during March and April 2001 [Jacob et al., 2003]. UWNMS forecasts were made for each DC-8 and P3 flight. These simulations were initialized with $1^\circ \times 1^\circ$ aviation model (AVN) forecasts from the National Centers for Environmental Prediction, together with ozone fields derived with the PV-mapping method of Pierce et al. [1999]. Each simulation was started 60 hours prior to the end of the scheduled flight and integrated with a 60 s time step. The domain was centered at 130°E , 30°N , with 90×90 horizontal and 55 vertical grid points, for a resolution of $55 \text{ km} \times 55 \text{ km} \times 400 \text{ m}$. Convective parameterizations were turned off; vertical motions were calculated explicitly. The horizontal boundaries of the UWNMS were updated every time step from 1.0° AVN forecast files every 6 hours. Rayleigh friction sponge layers were applied near the top (22 km) and sides of the domain to suppress spurious wave reflection.

[12] Model variables were archived every 5 min for diagnosis using VIS-5D visualization software [Hibbard and Santek, 1989]. An idealized tracer was initialized to decrease linearly everywhere from 1 at the surface to 0 at the top. This was useful for visualizing transport associated with convection and synoptic-scale flows. The idealized tracer and ozone were treated as conserved quantities. VIS5D output included 3D winds, pressure, temperature, potential temperature, potential vorticity, perturbation equivalent potential temperature, water vapor mixing ratio, precipitable water content, idealized tracer, and ozone.

2.3. TRACE-P Validation Data Sets

[13] Images from infrared, visible, and water vapor channels on Japan's Geostationary Meteorology Satellite 5 (GMS-5), together with meteorological analyses and trajectories created by TRACE-P science team members, were obtained during the campaign. Time-altitude sections of Langley differential absorption lidar (DIAL) ozone [Browell et al., 2003] and in situ ozone [Avery et al., 2001] (see http://www-gte.larc.nasa.gov/trace/TP_Avery_Vay_Instrument.htm and http://cloud1.arc.nasa.gov/solvell/instrument_files/O3.pdf) for DC-8 flight 14 are used to compare with ozone features seen in the UWNMS.

3. UWNMS Forecast for DC-8 Flight 14 on 24 March

[14] The UWNMS forecast for the DC-8 flight on 24 March was integrated for the 66 hours 0000 UT 22 March to 1800 UT 24 March. It showed the development of a convective complex over eastern China and subsequent propagation eastward into a region observable by the DC-8. This presented an opportunity to evaluate how deep convection redistributes and modifies continental and marine air transported from the boundary layer. By 4:00 P.M. local time 23 March GMS satellite imagery confirmed the convective development. A secondary goal was added for flight 14, to measure the convective complex. The primary goal was to sample carbon monoxide in cloud-free air to compare with

MOPITT instrument satellite overflight observations [Kiley et al., 2003]. Flight 14 lasted from 2310 UT 23 March to 0820 UT 24 March (8:10 A.M. to 5:20 P.M. local time).

[15] Figure 1 shows GMS-5 enhanced infrared images for a sequence of times during the convective event. At 0631 UT 23 March (3:31 P.M. local time) the convective complex was near 30°N , 115°E , appearing as a blue area approximately $500 \text{ km} \times 500 \text{ km}$ in Figure 1a, with cloud top temperatures near -50°C . The area of high clouds expanded with time, reaching $\sim 1500 \text{ km} \times 700 \text{ km}$ 24 hours later (Figure 1d). Note the development of the storms over the Pacific and in western China, each effective mixing agents for dispersing constituents globally.

[16] Figures 2–4 show the UWNMS forecast for 23 March. At 2200 UT 23 March (7:00 A.M. local time 24 March) the sea level pressure distribution showed a weak high centered over central Japan, with a northeast-southwest oriented band of low pressure over northeast China (Figure 2). A low-pressure center near the east coast of China coincided with the region of convection seen in the infrared satellite image in Figure 1b. Moist boundary layer air from southern China (orange) was predicted to ascend along the 300 K surface northeastward into the convective region (Figure 2).

[17] Figure 3 shows an east-west section through the convective region and the sea level pressure distribution (black contours) at 0300 UT 24 March (noon local time). The surface low was forecast to be located south of Japan, with upward motions exceeding 0.3 m s^{-1} (pink) at its eastern edge. The idealized tracer initialized to be 1 at the surface (orange) and 0 at the top (deep blue) suggested the ventilation of moist, polluted boundary layer air into the upper troposphere, with detrainment out its eastern edge near the tropopause. Note the signature of descending stratospheric air (green) around the periphery of the convection. UWNMS ozone values of ~ 100 ppbv were forecast near 6 km to the east of the convection (not shown). On the basis of this forecast it was anticipated that a spiral ascent into the convective outflow might yield a chemical signature of interaction with hydrometeors [e.g., Cohan et al., 1999].

[18] Potential temperature contours (black) in Figure 3 suggested that the tropopause near 340 K would be deformed upward over the convection. Above the convective updraft, coherent undulations may be seen in the potential temperature contours tilting westward with height, indicating upward and westward propagation of gravity wave energy away from the convective source. Individual wave crests moved westward and downward with time relative to the convection (not shown). Horizontal and vertical wavelengths are estimated to be $\sim 1000 \text{ km}$ and $\sim 10 \text{ km}$, giving a westward intrinsic trace speed of $\sim 30 \text{ m s}^{-1}$. Such waves tend to break because of Kelvin-Helmholtz instability, leading to mixing in the lowest stratosphere [e.g., Sato, 1994; Alexander and Pfister, 1995].

[19] A horizontal slice at 12.5 km in the UWNMS forecast for 0400 UT (1:00 P.M. local time) 24 March predicted that the convective complex would penetrate vertically through the subtropical westerly jet (Figure 4). The 53 m s^{-1} isosurface is shown in light purple, indicating that some of the strong westerly flow is deflected northward around the complex. Note the low PV in the deflected tropospheric jet. The rapid eastward progression of the

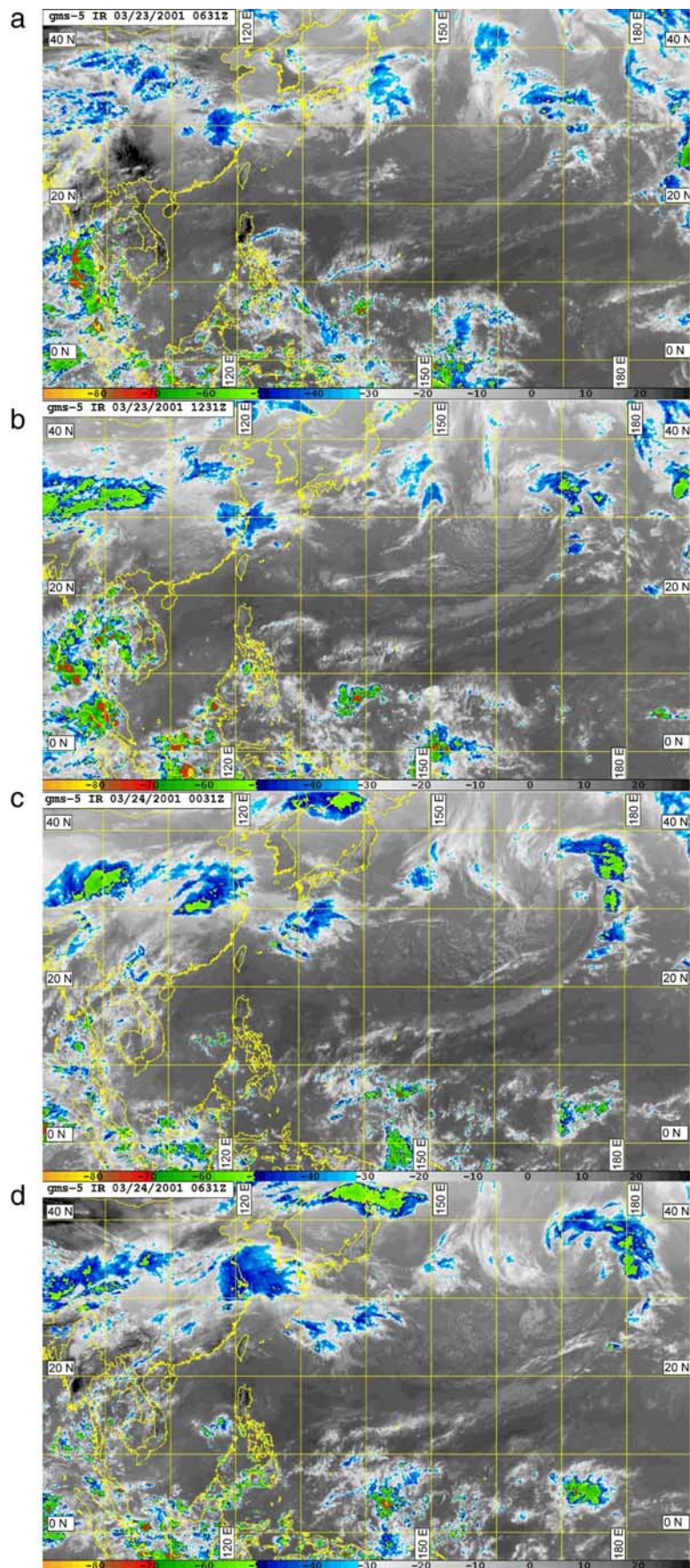


Figure 1

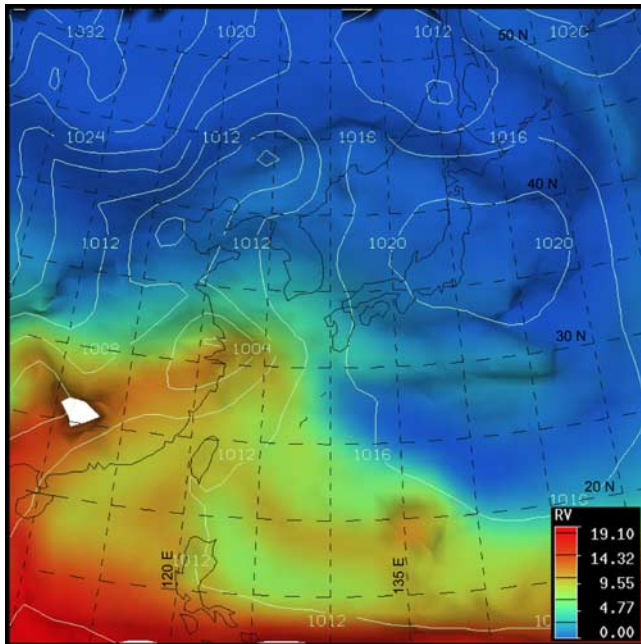


Figure 2. University of Wisconsin Nonhydrostatic Modeling System (UWNMS) forecast for 2200 UT on 23 March 2001 (7:00 A.M. on 24 March local time), showing sea level pressure (white contours, interval 4 hPa) and water vapor mixing ratio on the 300 K potential temperature surface (g kg^{-1} , color bar). High water vapor values, indicative of southeast China urban boundary layer air, are advected northeastward and upward ahead of the surface low.

convection is due to being imbedded in this westerly jet. This roughly cylindrical convective updraft created a form drag, representing a westward torque on the subtropical westerly jet, an extratropical example of “cumulus friction” [Schneider and Lindzen, 1976].

4. Flight 14 Observations

[20] Figures 1b–1d depict the east-southeastward progression and weakening of the convective complex over the Pacific. It reached the coast of China by 1231 UT (9:31 P.M. local time) on 23 March (Figure 1b). About an hour after the DC-8 took off the next morning the convective system was still strong and centered south of Japan (0031 UT, 9:31 A.M. local time on 24 March (Figure 1c)). Six hours later when the aircraft flew through the system, it had weakened and spread out (0631 UT, 3:31 P.M. local time on 24 March (Figure 1d)). Approaching the system one could see multiple layers of diffuse clouds without any distinct visual center to the system.

[21] Figure 5 shows the flight track superimposed on a GMS-5 infrared image at 0332 UT (12:32 P.M. local time).

A thin layer of high ozone was seen near 6.5 km altitude on the ozone sensor readout during the ascent at \sim 0040 UT (9:40 A.M. local time), possibly indicative of a stratospheric intrusion. Near 0205 UT (11:05 A.M. local time) no cirrus was observed overhead as the plane circled downward, taking a carbon monoxide profile for comparison with the MOPITT overpass. At \sim 0430 UT (1:30 P.M. local time) the DC-8 entered a stratocumulus deck at 1200 m. By 0520 (2:20 P.M. local time) clouds were seen overhead at \sim 4–6 km. Near 0545 UT (2:45 pm local time) lightning was detected 150 km to the east, indicating a cluster of thunderstorms that were still active, embedded within the broader cloud mass. At 0617 UT (3:17 P.M. local time) the aircraft began a spiral ascent through air with relatively low amounts of ozone, holding near 8 km (24,000 feet) below an aircraft aloft. Ascent resumed heading northbound, to 11 km (33,000 feet) by 0720 UT (4:20 P.M. local time), with cirrus clouds observed overhead near 12 km.

[22] The Langley DIAL ozone data for this flight are shown in Figure 6. Values less than 40 ppbv were seen in the marine boundary layer. Values exceeding 100 ppbv were seen above 12 km during the first 2 hours and last hour of the flight, corresponding to times when the aircraft was farthest north, detecting extratropical stratospheric ozone. During the first 2 hours ozone amounts exceeding 80 ppbv were seen near 6 km, with a layer of ozone-poor air between 7 and 10 km. UWNMS results suggest that this structure resulted directly from the convective transport of high ozone down to 6 km around its periphery, with detrained low ozone centered near 9 km. Owing to the presence of clouds the DIAL did not sense the upper troposphere during 0430–0630 UT.

[23] DC-8 flight altitude and in situ ozone mixing ratio are shown as a function of time in Figure 7. Near 0040 UT at 6.5 km a spike of 100 ppbv ozone was observed. Near 0200 and 0400 UT the aircraft was at or above 8 km, with ozone values exceeding 80 ppbv. During 0630–0730 UT ozone decreased below 70 ppbv within the convective complex and its outflow in the layer 8–10 km. On descent into Yokota a spike of \sim 80 ppbv ozone was seen at 5 km near 0750 UT.

[24] Ozone mixing ratio is presented as a function of altitude in Figure 8 for six flight segments during which substantial ascent or descent occurred. The locations may be inferred from the times labeled on Figure 5. These include ascent from Yokota (Figure 8a), descent near 28°N , 150°E (Figure 8b), ascent near 26°N , 150°E for the MOPITT underpass (Figure 8c), descent near 22°N , 142°E (Figure 8d), ascent in the convective complex near 28°N , 136°E (Figure 8e), and descent into Yokota (Figure 8f). Figure 8a shows a layer of enhanced ozone near 6.5 km during the ascent from Yokota, peaking at 100 ppbv, with a vertical half-width for the anomaly of \sim 500 m. Figures 8b–8d show ozone exceeding 80 ppbv above 8 km. Figure 8e shows less than 70 ppbv ozone close to the convective complex above 8 km. For the time shown in Figure 8e, the

Figure 1. GMS-5 satellite image of broadband infrared emission (converted to brightness temperature) at (a) 0631 UT on 23 March 2001, (b) 1231 UT on 23 March 2001, (c) 0031 UT on 24 March 2001, and (d) 0631 UT on 24 March 2001. Cloud top temperatures of \sim –50°C are associated with the convective complex, which propagated eastward from eastern China to southeast of Japan.

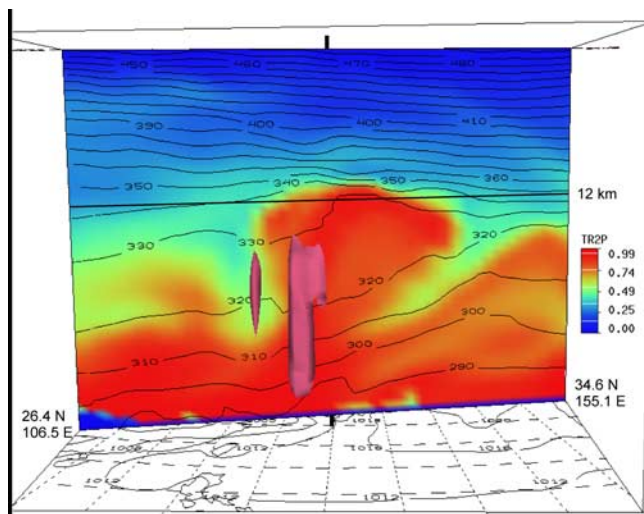


Figure 3. UWNMS forecast for 0300 UT on 24 March 2001 (11:00 A.M. on 24 March local time), showing sea level pressure (black contours, interval 4 hPa) and a vertical section with potential temperature (black contours, interval 10 K), the 0.3 m s^{-1} vertical velocity isosurface in pink, and the passive tracer initialized to be 1 at the surface (red) to 0 at 22 km (dark blue).

temperature and dew point (not shown) were equal to each other from 500 to 6500 m, confirming that the aircraft was within the clouds. Another narrow spike of high ozone was seen near 5 km in Figure 8f on descent to Yokota. The ozone spikes in Figures 8a and 8f coincided with layers of

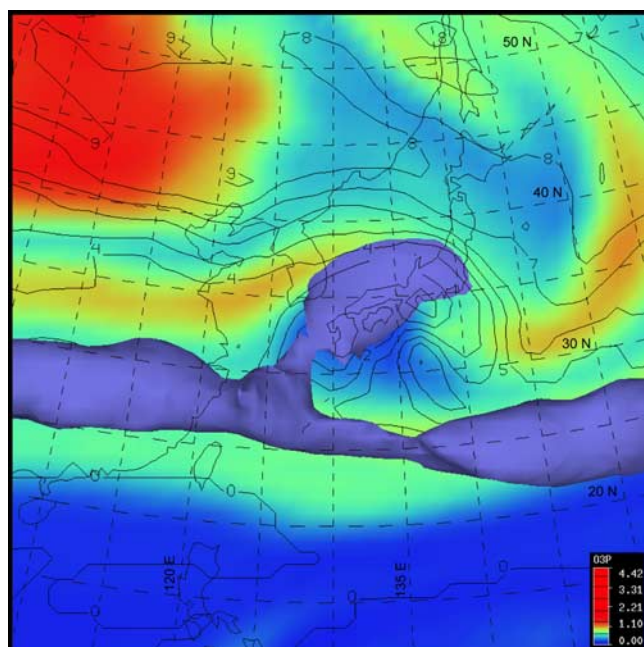


Figure 4. UWNMS forecast for 0400 UT on 24 March 2001 (1:00 P.M. local time), showing a horizontal slice at 12.5 km altitude of ozone in ppmv (color bar) and potential vorticity (black contours, 1 potential vorticity unit (PVU) interval). The 53 m s^{-1} isosurface of the subtropical westerly jet is shown in light purple.

anomalously low dew point (not shown). These observations are interpreted in the context of a higher-resolution UWNMS simulation in section 5.

5. UWNMS Hindcast for 24 March

[25] The two-scale method for evaluating the flux of material across PV surfaces was developed after the TRACE-P mission. To more accurately diagnose the case of 24 March a UWNMS hindcast was made at 30 km resolution. The period of integration and domain size ($5000 \times 5000 \text{ km}$) was the same as for the forecast described in section 3. Cross-tropopause ozone flux was calculated with the two-scale method for a range of applications of the bidirectional 1-2-1 filter. Results are shown for a frequency response of 10% at 500 km and 60% at 1000 km scales. Thus the convective complex is regarded as part of the motions which contribute to STE.

[26] Figure 9 shows the horizontal distribution of ozone at 6.5 km and a vertical section along the flight track at 0100 UT (10 A.M. local time). Values less than 50 ppbv are seen in the model over the southeastern tip of Japan, with values of ~ 100 ppbv near the flight track. The vertical section shows that the DC-8 flew through a downwelling plume of stratospheric air which curved westward toward the convective center near 6.5 km, reminiscent of a wide variety of numerical simulations and observations of the circulation near a warm bubble. It resembles the downwelling circulation around a nuclear explosion or the shape of a jellyfish (medusa). The modeled region of 40–50 ppbv ozone in the layer 8–12 km agrees in location and value with the layer of reduced ozone in the DIAL observations (compare Figures 9b and 6). Note also the westward tilting

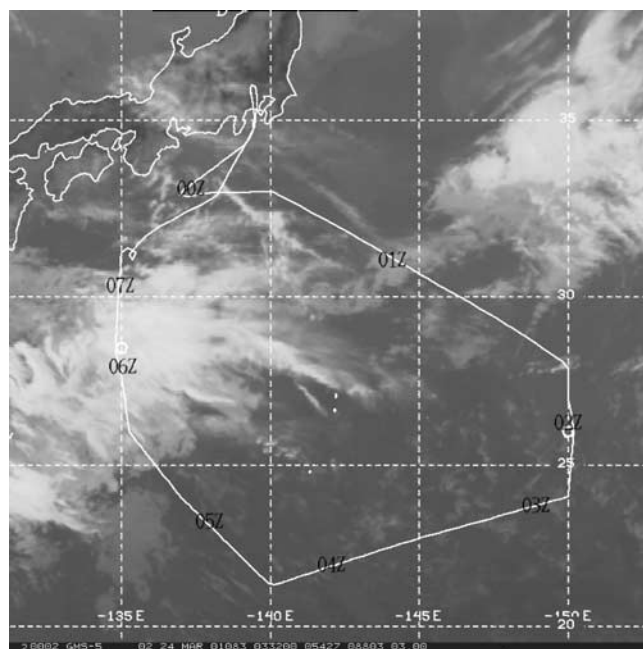


Figure 5. Horizontal projection of DC-8 TRACE-P flight 14 during 2330 UT on 23 March to 0830 UT on 24 March 2001 (8:30 A.M. to 5:30 P.M. local time), superimposed on an infrared image from the GMS-5 satellite at 0332 UT (12:32 P.M. local time).

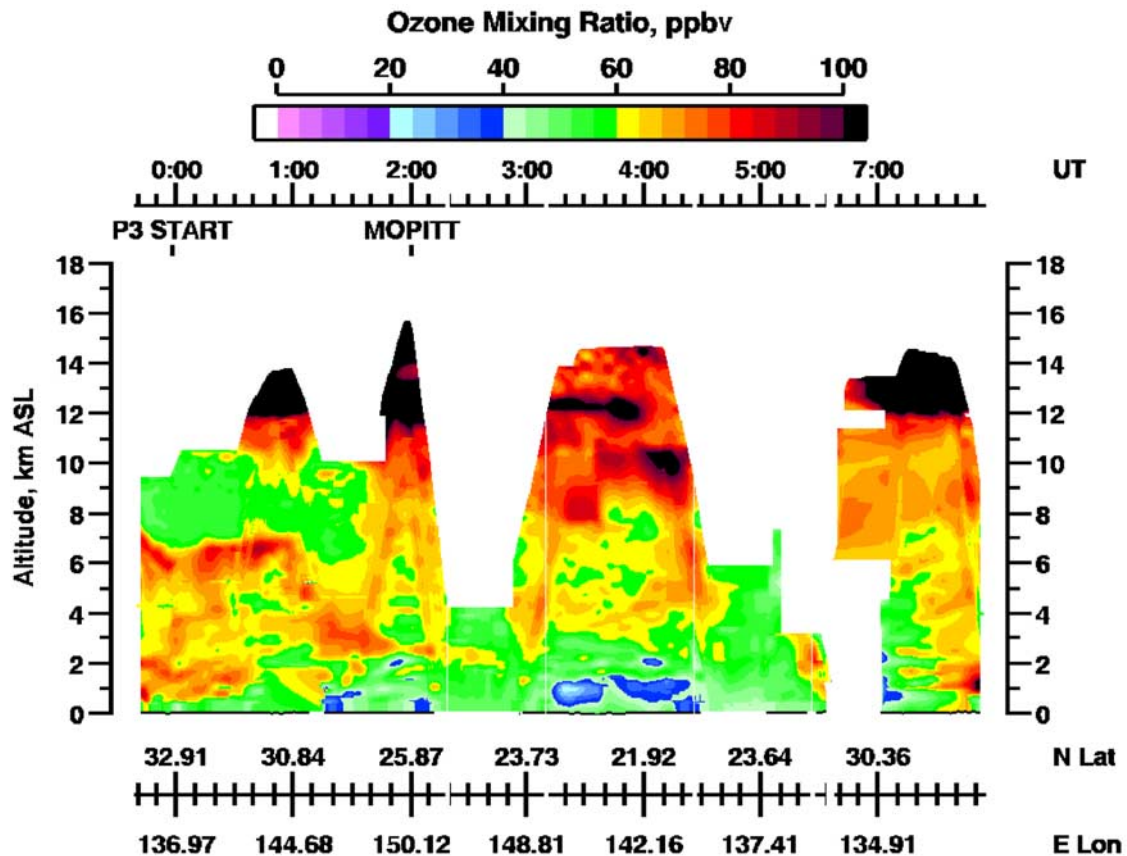


Figure 6. Time-height section of Langley DIAL ozone mixing ratio in ppbv for flight 14. Note the break in time near 0600 UT when the plane was in the clouds.

inertia-gravity waves in the ozone pattern in the stratosphere downstream of the convection, suggestive of strong disturbances ahead of the rapidly moving convective tops and imminent mixing of air in UTLS (Figure 9b).

[27] Figure 10 shows the horizontal distribution of ozone at 9 km and a vertical section along the flight track at 0700 UT (4 P.M. local time). The region of 40–50 ppbv ozone in the 8–12 km layer above the flight track has moved eastward. From ~0650 to 0700 UT the aircraft was ascending through air with ozone ~75 ppbv, diluted stratospheric air curling downward and westward to the east of the convective plume. After 0700 UT the plane ascended into the updraft vault containing lower ozone (Figures 8e and 10b). The vertical section further illustrates the evolving downwelling plumes of high ozone around the updraft of ozone-poor air in this aging convection. Entrainment of stratospheric air in the middle troposphere likely contributed to the decay of the storm.

[28] UWNMS 10 km streamlines and ozone flux for 0100 UT (10 A.M. local time) are shown in Figure 11a. Note the poleward redirection of the westerly jet around the convection region. The radius of the disturbed region exceeds 1000 km. Dashed lines indicate downward ozone flux of order $1\text{--}4 \times 10^{12}$ molecules $\text{cm}^{-2} \text{s}^{-1}$, which occurs near the west, southeast, and northeast edges of the convection.

[29] Figure 11b shows a longitude-altitude section of UWNMS stream function in the plane, PV contours (black) and ozone flux (dashed lines) at 0400 UT (1 P.M. local

time) on 24 March. High values of PV are seen on the periphery of the convection and also in the lower portions of the convection. The latter is due to latent heating maximizing in the middle troposphere, increasing the static stability, hence PV, in the lower troposphere. The streamlines show the rapid ascent of boundary layer air and detrainment at upper levels. Downward extension of stratospheric air is seen around the periphery, coinciding with a flux of ozone into the troposphere on the order of $1\text{--}4 \times 10^{12}$ molecules $\text{cm}^{-2} \text{s}^{-1}$. The stratospheric intrusion to the east of the convection is located farther away from the convective

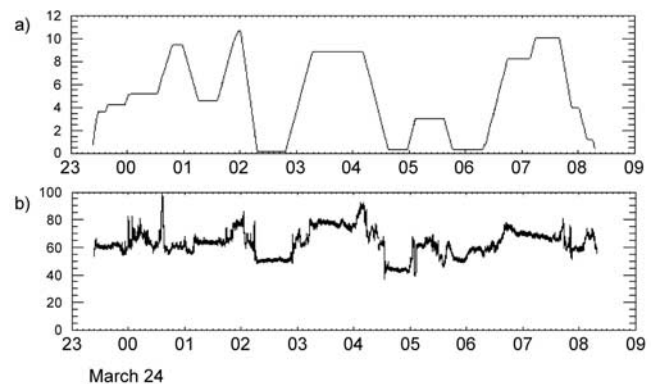


Figure 7. (a) Flight altitude (km) and (b) in situ ozone mixing ratio (ppbv) on flight 14.

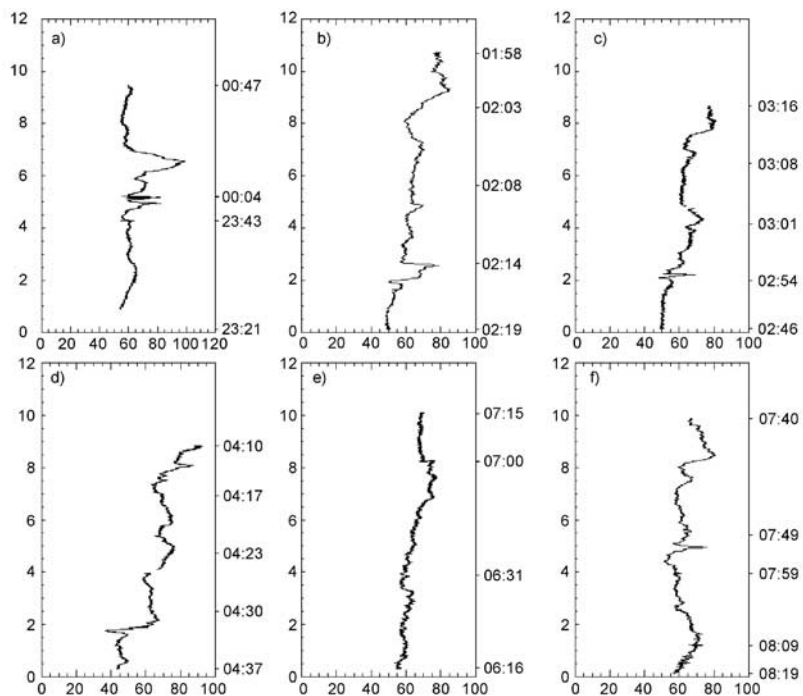


Figure 8. Ozone at flight level (ppmv) shown as vertical profiles for the periods (a) 2328 UT 23 on March to 0047 UT on 24 March ascent from Yokota, (b) 0158–0219 UT on 24 March, descent near 28°N, 150°E, (c) 0246–0316 UT on 24 March, ascent near 26°N, 150°E for MOPITT underpass, (d) 0410–0437 UT on 24 March, descent near 22°N, 142°E, (e) 0616–0715 UT on 24 March, ascent in the convective complex near 28°N, 136°E, and (f) 0740–0819 UT on 24 March, descent into Yokota.

center because of the detrainment of tropospheric air into the westerly jet.

[30] Figure 12 shows the history of net ozone flux across the 1.3 potential vorticity unit surface ($10^{-6} \text{ m}^2 \text{ K kg}^{-1} \text{ s}^{-1}$),

integrated over the model domain for the entire simulation. An initial model dynamical adjustment is seen during the first hour, then the ozone flux varies around -1×10^{28} ozone molecules s^{-1} for the first 36 hours. From 1200 UT

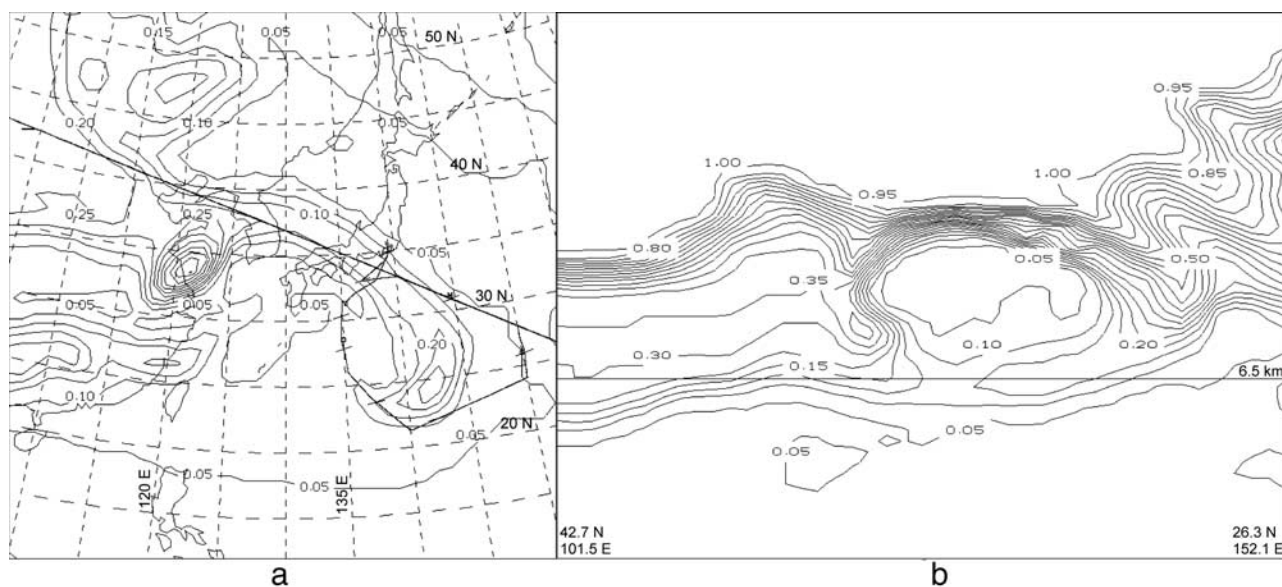


Figure 9. UWNMS ozone simulated at 30 km resolution for 0100 UT on 24 March 2001 (10 A.M. local time), with contour interval of 50 ppbv: (a) horizontal section at 6.5 km and (b) vertical section parallel to flight track, with a view toward the north.

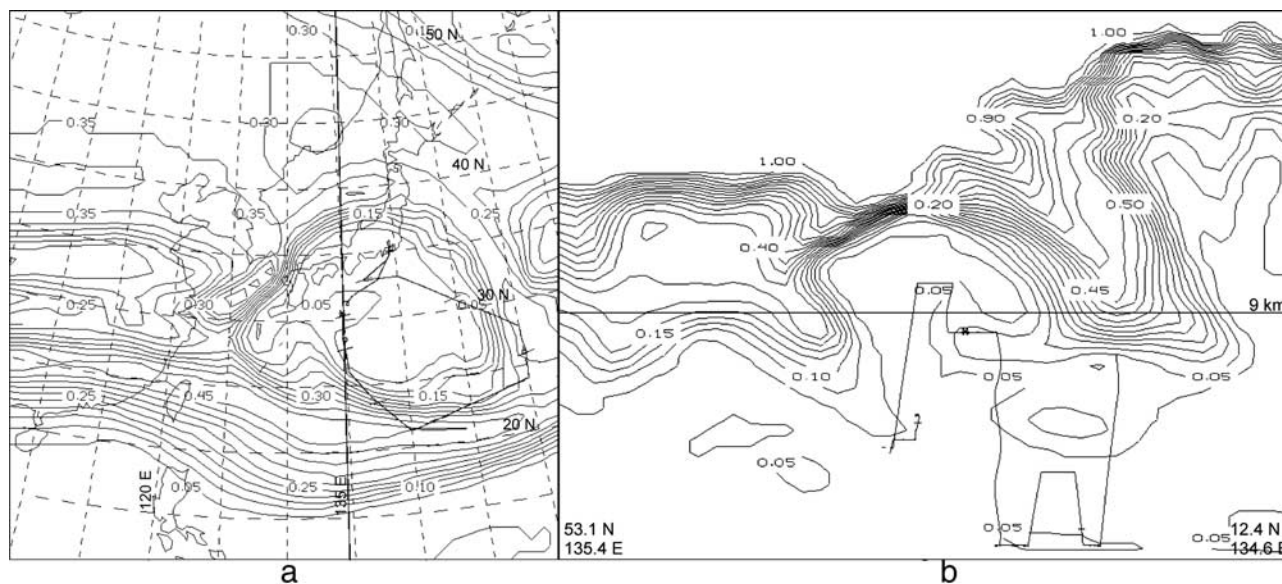


Figure 10. As in Figure 9, except for 0700 UT on 24 March 2001 (4 P.M. local time) and (a) horizontal section at 9 km and (b) vertical section parallel to flight track, with a view toward the east.

on 23 March to 0000 UT on 24 March the flux averaged -5×10^{28} ozone molecules s^{-1} . On 24 March the ozone flux averaged -1×10^{29} ozone molecules s^{-1} .

[31] An idealized calculation may be made for comparison. Assume that an annulus of 100 ppbv ozone with inner and outer radii 1000 and 1500 km, extending from 5 to 10 km altitude, is irreversibly mixed into the troposphere over a 24 hour period. Then $\sim 10^{29}$ ozone molecules s^{-1}

(10^{34} molecules d^{-1} or 0.8 Tg ozone d^{-1}) will enter the troposphere over this 5000×5000 km domain, similar in magnitude to results from the two-scale method. This is comparable to the downward averaged flux across 7 km altitude over East Asia reported by Carmichael *et al.* [1998] during early May 1987. Kentarchos *et al.* [2000] found values of ~ 1 Tg d^{-1} for synoptic cyclones. Buker *et al.* (submitted manuscript, 2004) applied the two scale

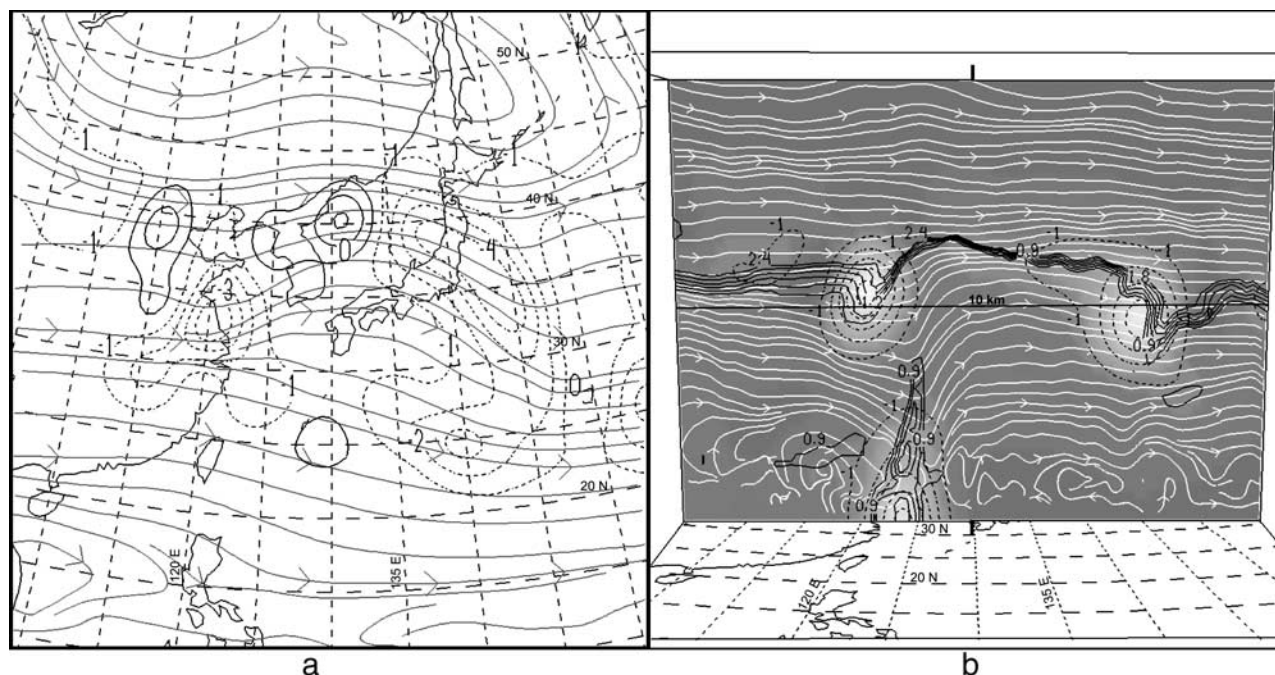


Figure 11. UWNMS simulation at 30 km resolution for 0400 UT on 24 March 2001 (1 P.M. local time): (a) 10 km streamlines and ozone flux (contour interval 1×10^{12} molecules $cm^{-2} s^{-1}$) and (b) streamlines in a vertical section through the convective complex, with potential vorticity (black contours from 0.9 to 2.4 PVU, with interval 0.3), and ozone flux. Note the ascent of boundary layer air to the upper troposphere in the convective complex and the downward ozone flux on the periphery.

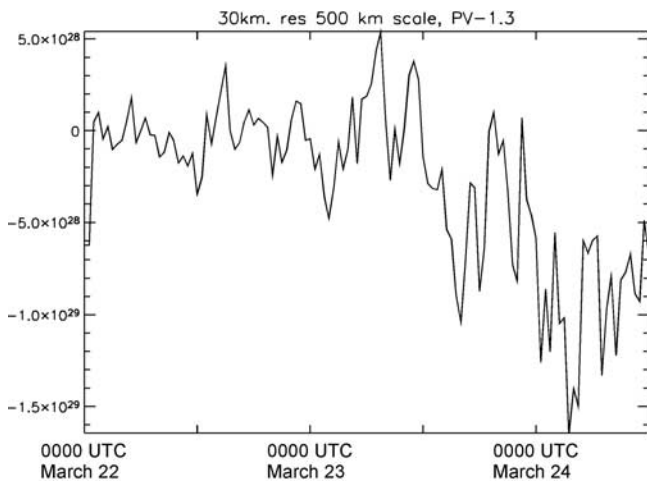


Figure 12. Time variation of horizontally integrated ozone flux across the 1.3 PVU surface for the 30 km UWNMS hindcast during 0000 UT March 22 to 1200 UT on 24 March 2001.

method to the synoptic cyclone on 26 March and obtained 0.13 Tg d^{-1} . Pierce *et al.* [2003] report an average ozone flux for the TRACE-P period of 0.2 Tg d^{-1} . Convective systems such as the present case can cause STE comparable to strong cyclogenesis.

6. Conclusions

[32] Aircraft sampling of the convective complex on 24 March 2001 provided a unique opportunity to study how it affected the distribution of climatologically important trace gases. Ozone fields from the RAQMS used to initialize the UWNMS provided a good representation of synoptic-scale ozone structure, while the UWNMS evolved mesoscale ozone features, including downwelling around the periphery of the convective complex. Specific features in the simulation agreed well with observations, including the 6.5 km 100 ppbv ozone filament from the stratosphere and the vault of lower ozone in the convective updraft at 8–12 km altitude. A detailed comparison of aircraft with the 30 km resolution UWNMS simulation supports the conclusion that significant amounts of ozone can enter the troposphere around the periphery of deep convection in the extratropics.

[33] The new two-scale method was applied to this convective situation which has the advantages of making use of resolved motions in the model and provides a new way to estimate viscous diabatic processes which transport material across the tropopause. Ozone STE was markedly enhanced during the lifetime of the convective event, with $\sim 10^{34}$ molecules d^{-1} entering the troposphere. The convection radiates inertia-gravity waves which further deform the ozone pattern. Langford *et al.* [1995] showed the seasonal evolution of volcanic aerosol over Colorado and argued that convective entrainment erodes the tropopause upward during summer. The present work suggests that STE associated with deep convection is a significant process which should be taken into account in the global budgets of ozone and other climatologically important trace species.

[34] **Acknowledgments.** We thank the TRACE-P science team for their careful measurements, planning, and analysis which made this work possible. We gratefully acknowledge support from NASA TRACE-P grant NCC1-01-011 and ACMAP grant NAG5-11303.

References

- Alexander, M., and L. Pfister (1995), Gravity wave momentum flux in the lower stratosphere over convection, *Geophys. Res. Lett.*, **22**, 2029–2032.
- Avery, M. A., D. J. Westberg, H. E. Fuelberg, R. E. Newell, B. E. Anderson, S. A. Vay, G. W. Sachse, and D. R. Blake (2001), Chemical transport across the ITCZ in the central Pacific during an El Niño–Southern Oscillation cold phase event in March–April 1999, *J. Geophys. Res.*, **106**, 32,539–32,553.
- Avissar, R., E. Eloranta, K. Gurer, and G. J. Tripoli (1998), An evaluation of the large eddy simulation option of the Regional Atmospheric Modeling System in simulating the convective boundary layer: A Fire case study, *J. Atmos. Sci.*, **55**, 1109–1130.
- Browell, E. V., et al. (2003), Large-scale ozone and aerosol distributions, air mass characteristics, and ozone fluxes over the western Pacific Ocean in the late winter/early spring, *J. Geophys. Res.*, **108**(D20), 8805, doi:10.1029/2002JD003290.
- Carmichael, G. R., I. Uno, M. J. Phadnis, Y. Zhang, and Y. Sunwoo (1998), Tropospheric ozone production and transport in the springtime in East Asia, *J. Geophys. Res.*, **103**, 10,649–10,671.
- Cohan, D. S., M. G. Schultz, D. J. Jacob, B. G. Heikes, and D. R. Blake (1999), Convective injection and photochemical decay of peroxides in the tropical upper troposphere: Methyl iodide as a tracer of marine convection, *J. Geophys. Res.*, **104**, 5717–5724.
- Danielsen, E. F., R. S. Hipskind, S. E. Gaines, G. W. Sachse, G. L. Gregory, and G. F. Hill (1987), Three-dimensional analysis of potential vorticity associated with tropopause folds and observed variations of ozone and carbon monoxide, *J. Geophys. Res.*, **92**, 2103–2111.
- Eckman, R. S., W. L. Grose, R. E. Turner, W. T. Blackshear, J. M. Russell III, L. Froidevaux, J. W. Waters, J. B. Kumer, and A. E. Roche (1995), Stratospheric trace constituents simulated by a three-dimensional general circulation model: Comparison with UARS data, *J. Geophys. Res.*, **100**, 13,951–13,966.
- Haynes, P., and J. Anglade (1997), The vertical-scale cascade in atmospheric tracers due to large-scale differential advection, *J. Atmos. Sci.*, **54**, 1121–1136.
- Haynes, P. H., and M. E. McIntyre (1990), On the conservation and impermeability theorems for potential vorticity, *J. Atmos. Sci.*, **47**, 2021–2031.
- Haynes, P. H., and W. E. Ward (1993), The effect of realistic radiative transfer on potential vorticity structures, including the influence of background shear and strain, *J. Atmos. Sci.*, **50**, 3431–3453.
- Hibbard, W. L., and D. Santek (1989), The VIS-5D system for easy interactive visualization, in *Proceedings of Visualization '90*, pp. 28–35, IEEE Comput. Soc. Press, Los Alamitos, Calif.
- Hitchman, M. H., M. L. Buker, and G. J. Tripoli (1999), Influence of synoptic waves on column ozone during Arctic summer 1997, *J. Geophys. Res.*, **104**, 26,547–26,563.
- Hitchman, M. H., M. L. Buker, G. J. Tripoli, E. V. Browell, W. B. Grant, C. Hostetler, T. J. McGee, and J. F. Burris (2003), Nonorographic generation of Arctic polar stratospheric clouds during December 1999, *J. Geophys. Res.*, **108**(D1), 8325, doi:10.1029/2001JD001034.
- Holton, J. R., P. H. Haynes, M. E. McIntyre, A. R. Douglass, R. B. Rood, and L. Pfister (1995), Stratosphere-troposphere exchange, *Rev. Geophys.*, **33**, 403–439.
- Hoskins, B. J., M. E. McIntyre, and A. W. Robertson (1985), On the use and significance of isentropic potential vorticity maps, *Q. J. R. Meteorol. Soc.*, **111**, 877–946.
- Jacob, D., J. H. Crawford, M. M. Kleb, V. S. Connors, R. J. Bendura, J. L. Raper, G. W. Sachse, J. C. Gille, L. Emmons, and C. L. Heald (2003), Transport and Chemical Evolution over the Pacific (TRACE-P) aircraft mission: Design, execution, and first results, *J. Geophys. Res.*, **108**(D20), 9000, doi:10.1029/2002JD003276.
- Johnson, D. R., T. H. Zapotocny, F. M. Reames, B. J. Wolf, and R. B. Pierce (1993), A comparison of simulated precipitation by hybrid isentropic sigma and sigma models, *Mon. Weather Rev.*, **121**, 2088–2114.
- Kentarchos, A. S., G. J. Roelofs, and J. Lelieveld (2000), Simulation of extratropical synoptic-scale stratosphere-troposphere exchange using a coupled chemistry GCM: Sensitivity to horizontal resolution, *J. Atmos. Sci.*, **57**, 2824–2838.
- Kiehl, J. T., and S. Solomon (1986), On the radiative balance of the stratosphere, *J. Atmos. Sci.*, **43**, 1525–1534.
- Kiley, C., et al. (2003), An intercomparison and evaluation of aircraft-derived and simulated CO from seven chemical transport models during the TRACE-P experiment, *J. Geophys. Res.*, **108**(D21), 8819, doi:10.1029/2002JD003089.

- Kittaka, C., et al. (2004), A three-dimensional regional modeling study of the impact of clouds on sulfate distributions during TRACE-P, *J. Geophys. Res.*, *109*, D15S11, doi:10.1029/2003JD004353.
- Langford, A. O., T. J. O'Leary, M. H. Proffitt, and M. H. Hitchman (1995), Transport of the Pinatubo volcanic aerosol to a northern midlatitude site, *J. Geophys. Res.*, *100*, 9007–9016.
- Mecikalski, J. R., and G. J. Tripoli (1997), Inertial available kinetic energy and the dynamics of tropical plume formation, *Mon. Weather Rev.*, *126*, 2200–2216.
- Pierce, R. B., J. A. Al-Saadi, T. D. Fairlie, J. R. Olson, R. S. Eckman, W. L. Grose, G. S. Lingenfelter, and J. M. Russell III (1999), Large-scale stratospheric ozone photochemistry and transport during the POLARIS campaign, *J. Geophys. Res.*, *104*, 26,525–26,545.
- Pierce, R. B., et al. (2003), Regional Air Quality Modeling System (RAQMS) predictions of the tropospheric ozone budget over East Asia, *J. Geophys. Res.*, *108*(D21), 8825, doi:10.1029/2002JD003176.
- Pokrandt, P. J., G. J. Tripoli, and D. D. Houghton (1996), Processes leading to the formation of mesoscale waves in the midwest cyclone of 15 December 1987, *Mon. Weather Rev.*, *124*, 2726–2752.
- Reid, S. J., and G. Vaughan (1991), Lamination in ozone profiles in the lower stratosphere, *Q. J. R. Meteorol. Soc.*, *117*, 825–844.
- Sato, K. (1994), A statistical study of the structure, saturation, and sources of inertia-gravity waves in the lower stratosphere observed with the MU radar, *J. Atmos. Terr. Phys.*, *56*, 755–774.
- Sato, K., and T. J. Dunkerton (2002), Layered structure associated with low potential vorticity near the tropopause seen in high-resolution radiosondes over Japan, *J. Atmos. Sci.*, *59*, 2782–2800.
- Schneider, E. K., and R. S. Lindzen (1976), A discussion of the parameterization of momentum exchange by cumulus convection, *J. Geophys. Res.*, *81*, 3158–3160.
- Shapiro, M. A. (1980), Turbulent mixing within tropopause folds as a mechanism for the exchange of chemical constituents between the stratosphere and troposphere, *J. Atmos. Sci.*, *37*, 994–1004.
- Shine, K. P. (1987), The middle atmosphere in the absence of dynamical heat fluxes, *Q. J. R. Meteorol. Soc.*, *113*, 603–633.
- Tripoli, G. J. (1992a), An explicit three-dimensional nonhydrostatic numerical simulation of a tropical cyclone, *Meteorol. Atmos. Phys.*, *49*, 229–254.
- Tripoli, G. J. (1992b), A nonhydrostatic numerical model designed to simulate scale interaction, *Mon. Weather Rev.*, *120*, 1342–1359.
- Wirth, V., and J. Egger (1999), Diagnosing extratropical synoptic-scale stratosphere-troposphere exchange: A case study, *Q. J. R. Meteorol. Soc.*, *125*, 635–655.

J. A. Al-Saadi, M. A. Avery, E. V. Browell, and R. B. Pierce, NASA Langley Research Center, Hampton, VA 23681, USA. (j.a.al-saadi@larc.nasa.gov; m.a.avery@larc.nasa.gov; e.v.browell@larc.nasa.gov; r.b.pierce@larc.nasa.gov)

M. L. Buker, M. H. Hitchman, and G. J. Tripoli, Department of Atmospheric and Oceanic Sciences, University of Wisconsin-Madison, 1225 W. Dayton Street, Madison, WI 53706, USA. (marcus@aos.wisc.edu; matt@aos.wisc.edu; tripoli@aos.wisc.edu)